Nitrile Reaction in High-Temperature Water: Kinetics and Mechanism

Bill Izzo, Cynthia L. Harrell, and Michael T. Klein
Dept. of Chemical Engineering, University of Delaware, Newark, DE 19716

The reaction pathways, kinetics and mechanisms underlying the hydrolysis of aliphatic and aromatic nitriles in high-temperature water (HTW) were investigated. The reaction products were the associated amides and carboxylic acids. Autocatalytic kinetics were observed and confirmed by experiment and analysis of the physical chemistry of the HTW reaction environment. A model incorporating two autocatalytic steps captured the observed kinetics well, and the associated optimized rate constants highlighted the key differences in the reaction chemistry of aliphatic and aromatic nitriles. The rate behavior of nitrile hydrolysis at these conditions has tangible consequences regarding optimal processing strategies.

Introduction

Reaction in near- and supercritical water has attracted considerable interest as a potential technology for the disassembly of toxic and energetic waste materials. Optimization of process vessels, reaction conditions, and possible additives can be facilitated by the development of quantitative information about the underlying reaction pathways, kinetics, and mechanisms. Nitriles command special attention because of their appearance in industrial-waste streams and in product spectra from the reaction of NO_2-containing aliphatics in high-temperature water (Iyer et al., 1996). This motivated the present study of the kinetics and mechanisms of acetonitrile and benzonitrile in high-temperature water.

The literature provides guidance in terms of the related investigations into the high-temperature reactions (> 100°C) of heteroatom-containing compounds. Most studies have focused attention on the overall destruction efficiencies, with less analysis of the underlying reaction pathways and quantitative kinetics. More specific study of nitriles in a hydrothermal environment is limited to the work by Katritzky and coworkers on benzonitrile and pyridinecarbonitriles (Katritzky et al., 1990). Two-phase benzonitrile hydrolysis at 250°C yielded the amide and carboxylic acid with some degree of decarboxylation of the acid. The pyridinecarbonitriles were more reactive relative to benzonitrile; rapid decarboxylation resulted in pyridine formation. Recently, Kuhlmann and coworkers found that both simple elimination and hydrolysis chemistry in high-temperature water parallel that observed at moderate temperatures (Kuhlmann et al., 1994).

The lower-temperature (< 100°C) kinetics and mechanisms of acid- and base-catalyzed nitrile hydrolysis have been investigated more extensively. Studies of the acid-catalyzed hydrolysis of aliphatic nitriles (Krieble and Noll, 1939; Rabinovitch and Winkler, 1942a; Rabinovitch et al., 1942; Wideqvist, 1956; Grigoryan et al., 1976) revealed that high concentrations of acid (> 11 N) are required to hydrolyze nitriles rapidly. Alkaline hydrolysis, in contrast, required lower concentrations of base to achieve an equivalent rate (Rabinovitch and Winkler, 1942b). The acid-catalyzed hydrolysis activation energy is approximately 5 kcal/mol higher than the base-catalyzed hydrolysis (Rabinovitch and Winkler, 1942b).

The goal of the currently described program was to contribute quantitative pathways, kinetics, and mechanisms to this literature, with the ultimate objective of specifying optimal conditions for the safe and socially acceptable disassembly of these and related compounds. Thus, the implications of the resolved pathways and kinetics on classic reactor design issues were also sought. This report focuses on the reactions in high-temperature water (250–300°C), where the quantitative needs are the greatest.

Experimental Section

Materials

The aqueous reaction chemistry of acetonitrile, acetamide, benzonitrile, and benzamide was investigated at tempera-

Correspondence concerning this article should be addressed to M. T. Klein.

tures from 250 to 300°C, at pressures from 40 to 87 bar and for batch holding times ranging from 10 to 225 min. Reactant concentrations spanned a range from 0.2 to 0.71 M. All chemicals were commercially available from Aldrich in purities of 98% or higher and were used as received.

The reactions were performed in closed, constant volume, and essentially isothermal microreactors. Two types of reactors were utilized. The benzonitrile and benzamide reactions were performed in 4.2 cm^3 reactors constructed from 316 stainless-steel (SS) 1/2-in. (12.7-mm) Swagelok port connectors and two 1/2-in. (12.7-mm) Swagelok caps. The acetonitrile and acetamide reactions were performed in 4.0 cm^3, 316 SS reactors manufactured by Trico Machine Products, Inc., based on a design by Autoclave Engineers.

Loadings were selected to ensure that the entire reactor volume was occupied by compressed liquid water. Saturated liquid densities at the desired reaction temperature were obtained from the steam tables. The operative reaction pressure was thus different for each temperature studied. As a benchmark, the pressure of saturated liquid water is 87 bar at 300°C.

Procedure

The experimental procedure reflected the safety concerns of using high temperature and pressures. A barricade equipped with a view window was installed. The procedure for loading the reactors was dependent on the type of reactor (or reactant). For acetonitrile and acetamide reactants, a typical experimental procedure began with the preparation of aqueous reaction solutions at room temperature. The reaction solution was loaded into the reactor, which was then sealed in a benchtop vise using a torque wrench to achieve a consistent sealing pressure. A 1-mm-thick titanium gasket was placed between the base and top of the reactor to create a leak-free seal. This loading procedure could not be extended to the benzonitrile and benzamide reactions due to immiscibility at ambient conditions. For these reactions, water and reactant were added individually to the reactor and the reactor sealed with standard wrenches. No further attempt was made to purge either reactor of air, as the reaction solution occupied a majority of the reactor volume. All loadings were verified with a Mettler AE200 balance (± 0.1 mg).

To carry out the reaction, the sealed reactors were placed into a steel basket, which was lowered into a preheated Techne fluidized sandbath maintained at the reaction temperature, ± 2°C, by an Omega temperature controller. Reactors were submerged approximately 6 in. below the surface of the sand. After the desired reaction time had elapsed (10–225 min), the reactors were removed from the sandbath and immersed in an ice/water bath to quench the reaction. Reactors were tested for leaks by weighing before and after each reaction. The soluble contents were then recovered in a single phase in HPLC-grade acetone. Reactors were triple rinsed with ~10 mL acetone. An external standard, biphenyl, was added for quantitative purposes.

Table 1. Experimental Conditions for Reactions in High-temperature Water*

Reactant	Structure	Temp. (°C)	Pres. (bar)	Reaction Time (min)
Benzonitrile	Ph**–CN	300	87	25–225
Benzamide	Ph**–$(CO)NH_2$	300	87	25–200
Acetonitrile	CH_3CN	300	87	15–180
Acetamide	$CH_3(CO)NH_2$	250	40	10–180

*Initial concentrations ranged from 0.2 to 0.71 M, corresponding to molar ratios [reactant]/[water] of 1/55 to 1/200.

**Ph = ◎.

Analytical chemistry

Product spectra were interpreted by GC/MS (HP Gas Chromatograph equipped with a 25/50-m HP-FFAP acid-modified polyethylene glycol capillary column coupled to an HP-5970 mass selective detector). The mass spectra were matched to a Wiley library, and assignments were subsequently confirmed by coinjection on an HP 5880 GC. Quantitative analysis was completed via GC using HP 5880/90 instruments equipped with a 50-m HP-FFAP acid-modified polyethylene glycol column for acetonitrile and acetamide runs and a 50-m HP Ultra 2 column for benzonitrile and benzamide runs. A flame ionization detector was used for quantitation of all reactants and products. Response factors were determined from analysis of prepared standard mixtures.

Experimental Results

Table 1 summarizes the experiments performed, which provided information about the global kinetics, the product spectra, and the quantitative yields within. In discussion of the results, a comparative analysis of the global kinetics for the two nitriles first sets the basis for subsequent scrutiny of product molar yields. This allows inference of the controlling reaction pathways and mechanisms.

Table 2 summarizes the observed product spectra. These relatively clean product spectra were dominated by the presence of amides and carboxylic acids. Thus at the reaction conditions of Table 1, the dominant reaction chemistry was the addition of water to the electrophilic carbon. This reaction is consistent with observations in the literature at near-ambient conditions (McMurry, 1984; Loudon, 1988; March, 1992) and can be represented by Eq. 1:

Table 2. Product Spectrum for Reaction of Nitriles in HTW

Reactant	Acetonitrile CH_3CN	Benzonitrile Ph–CN	Acetamide $CH_3(CO)NH_2$	Benzamide Ph–$(CO)NH_2$
Primary products	Acetamide $CH_3(CO)NH_2$	Benzamide Ph–$(CO)NH_2$	Acetic acid Ammonia	Benzoic acid Ammonia
Secondary products	Acetic acid $CH_3(CO)OH$ Ammonia NH_3	Benzoic acid Ph–$(CO)OH$ Ammonia NH_3		

$$R-C\equiv N \xrightarrow{H_2O} R-\overset{O}{\overset{\|}{C}}-NH_2 \xrightarrow{H_2O} R-\overset{O}{\overset{\|}{C}}-OH + NH_3. \quad (1)$$

The first step of Eq. 1 involves the addition of water to the cyanogen group that yields the amide. This reaction product can then undergo a secondary hydrolysis to yield the carboxylic acid and ammonia. This represents the overall stoichiometry of the observed reactions. The actual form of the carboxylic acid and ammonia will depend on the physical chemistry of the system (ionization constant of the acid, basicity of the ammonia, and the ion product of water at the reaction conditions). The dominant form of these reaction products is investigated below.

Figure 1a shows the kinetics of benzonitrile conversion at 300°C. A conversion of 96% was obtained at the longest reaction time of 225 min. Figure 1b shows that nearly complete conversion of acetonitrile was obtained in a reaction time of 180 min. at 300°C. Best-fit model predictions for first-, second- and half-order kinetics are also included in Figures 1a and 1b. The kinetics for acetonitrile show significant deviation from first-, second-, and half-order kinetics. For benzonitrile, significant deviation is observed for first- and second-order kinetics. Although global half-order kinetics provides a reasonable account of the disappearance kinetics for benzonitrile, the analysis to follow will show that this global model fails to capture the observed product spectra. In both the acetonitrile and benzonitrile data, the rate of disappearance of the nitrile appears to increase with increasing reaction time, suggesting autocatalytic kinetics for these reaction systems.

Figures 2a and 2b show the time dependence of the product spectrum from reaction of benzonitrile and acetonitrile,

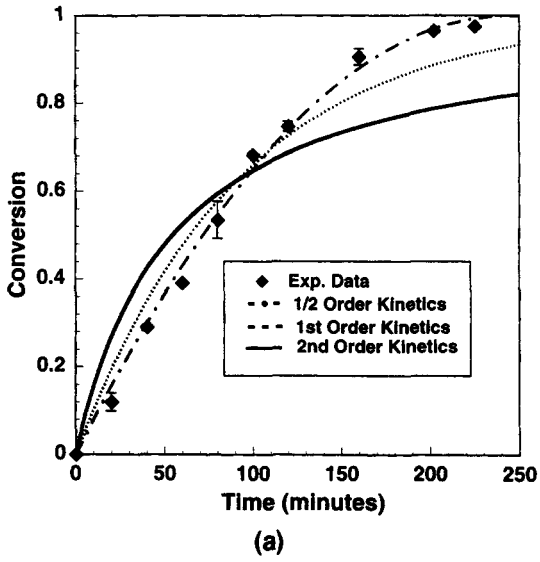

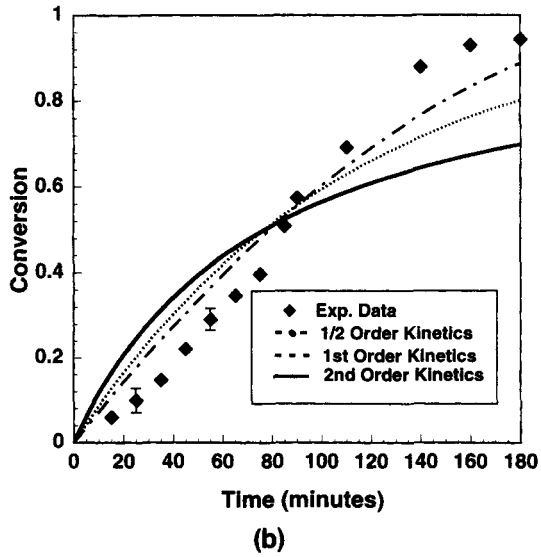

Figure 1. HTW reaction kinetics at 300°C and 87 bar: (a) for benzonitrile; (b) for acetonitrile.

♦, experimental data; — · —, one-half order; – – –, first order; ——; second order.

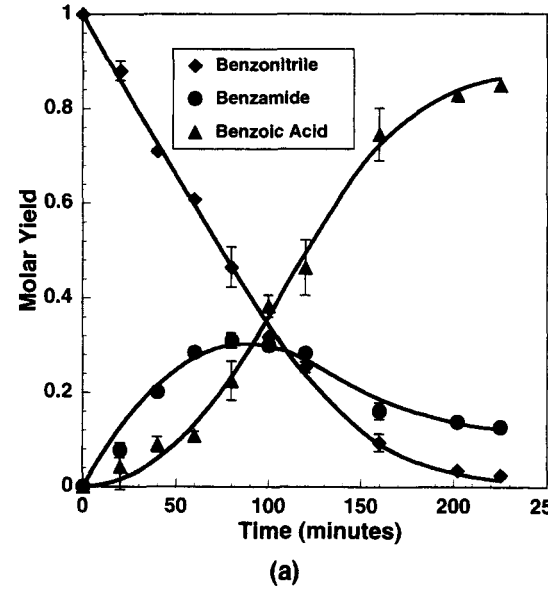

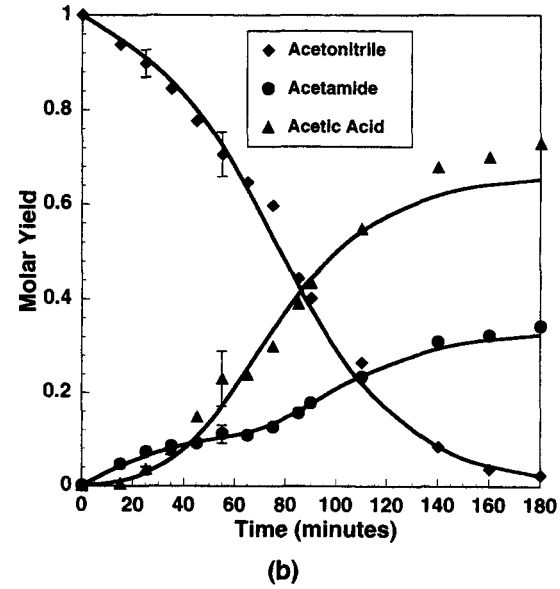

Figure 2. Time dependence of molar yields at 300°C and 87 bar: (a) for reaction of benzonitrile; (b) for reaction of acetonitrile.

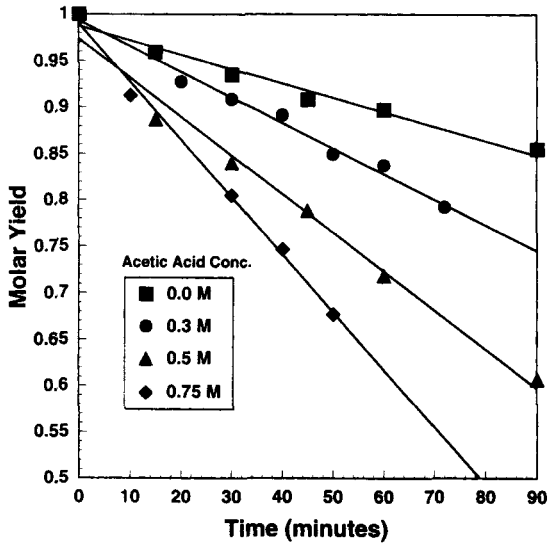

Figure 3. Acid-catalyzed acetonitrile hydrolysis at 250°C and 40 bar: variation of rate with initial acetic acid concentration.

respectively. The major short-time product was the amide. The dominant reaction product at long times was the carboxylic acid. The ratio of the yield of benzamide to that of benzoic acid was approximately 3 at 60-min reaction time. The ratio of the yield of acetamide to that of acetic acid was approximately 0.6 at 20-min reaction time. The autocatalytic behavior noted earlier is also evident in Figures 2a and 2b, which further highlight the increase in the rate of disappearance of the nitrile coinciding with the accumulation of the carboxylic acid. Thus, the autocatalytic agent may well be the final reaction product.

The significance of autocatalysis during nitrile hydrolysis was probed through a series of rate measurements which were made with varying initial acetic acid concentrations. Low conversion experiments nearly eliminated secondary hydrolysis

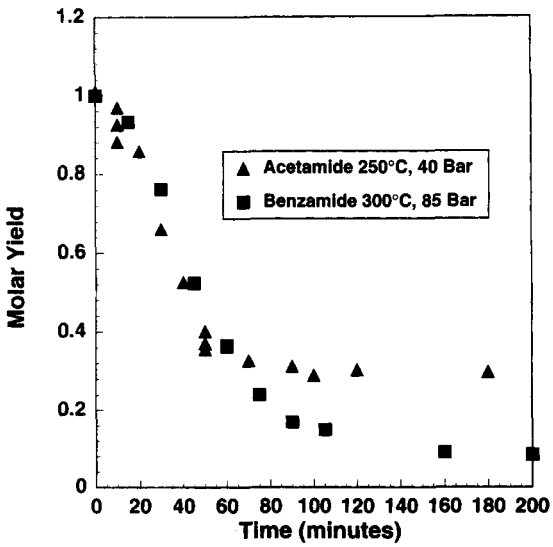

Figure 4. Disappearance kinetics for acetamide and benzamide in HTW.

of the nitrile and maintained a nearly constant concentration of carboxylic acid. Figure 3 shows a clear enhancement of the hydrolysis rate due to the presence of acetic acid (concentrations ranging from 0 to 0.75 M). Initial rate analyses showed the reaction to be first order with respect to acid concentration.

The reaction network was probed further through experiments conducted with the amides as the starting reactants. The results are shown in Figure 4 in the form of molar yield vs. time. The reactivity of benzamide at 300°C was similar to that for benzonitrile. The conversion of benzamide appeared to approach a thermodynamic equilibrium at longer times. Acetamide hydrolysis was much faster than benzamide hydrolysis, necessitating a lower reaction temperature (250°C) to obtain measurable kinetics. Figure 4 shows that the conversion of acetamide reached 70% after 90 min. This conversion was maintained for a reaction time of 180 min, indicating the possibility of a thermodynamic equilibrium. Qualitative calculations performed using a predictive Soave–Redlick–Kwong equation of state confirmed that complete conversion of the amide is not achieved at reaction conditions.

Reaction Network and Modeling Approach

The foregoing experimental data suggest complex kinetics for the hydrolysis of both nitriles and their reaction products. Evidently, one or more of the reaction products catalyzed the nitrile hydrolysis. This suggests the pathway-level reaction model shown in Figure 5. The source of the catalytic activity is not specified in Figure 5, although results from the acetic acid runs clearly demonstrate the dependence of the rate on the carboxylic acid concentration.

Complex reaction mechanisms involving multiple equilibrated proton transfer steps are common in aqueous chemistry and can lead to a variety of observed rate behaviors, depending on the presence of catalysts and the controlling elementary steps. The pathway-level reaction scheme of Figure 5 provides a starting point for analysis of the nitrile reaction kinetics. Figure 5 suggests the rate equation shown as Eq. 2a for nitrile disappearance, where R = CH_3 or C_6H_5:

$$-r_{\text{Nitrile}} = k_1[H_2O][R-CN] + k_3[H_2O][\text{Cat}][R-CN]. \quad (2a)$$

Similarly for amide hydrolysis:

$$-r_{\text{Amide}} = k_2[H_2O][R-C(O)NH_2] + k_4[H_2O][\text{Cat}][R-C(O)NH_2] - k_5[\text{Cat}][R-C(O)OH][NH_3]. \quad (2b)$$

Several species in the reaction mixture are potential catalysts (Cat in Eq. 2) for nitrile and amide hydrolysis. The nitrile reaction mixture contains, in general, five molecular species: nitrile, amide, carboxylic acid, ammonia, and water, the latter serving as both solvent and reactant. These species can further interact with the solvent to produce their conjugate acid or base forms, and in doing so alter the hydronium ion concentration in solution. This leads to five possible catalytic species: H_3O^+, *HA* (undissociated acid), NH_4^+, A^- (dissociated acid), and NH_3 and results in the following expansion for the catalytic terms in Eqs. 2a and 2b:

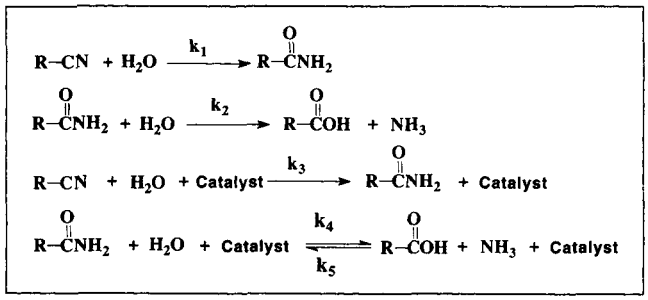

Figure 5. Pathway-level model for reaction of nitriles in HTW.

$$k_{3\text{ or }4}[\text{Cat}] = k_{H_3O^+}[H_3O^+] + k_{HA}[HA] + k_{NH_4^+}[NH_4^+] + k_A[A^-] + k_{NH_3}[NH_3]. \quad (3)$$

The first term represents the dependence of the reaction rate on the hydronium ion concentration (H_3O^+). This specific acid activity is independent of the structure of the proton donors present in the reaction mixture. The subsequent terms account for general acid/base catalysis, arising from Brönsted acids, acting as proton donors, and Brönsted bases, acting as proton acceptors. In this case, the rate is dependent on both the nature and concentration of the species involved in the reaction. More quantitative specification of the catalytic activity, that is, the concentrations and relative importance of the species in Eq. 3 requires a closer inspection of the physical chemistry of the system at high temperature and pressure reaction conditions.

Physical Chemistry of Reaction System

The kinetic scheme of Figure 5 and the pseudo-second-order catalytic rate constant of Eq. 3 motivated a detailed description of the physical chemistry of aqueous solutions at conditions of high temperatures and pressures. This was aimed at producing quantitative information concerning the acid/base equilibria at both ambient conditions and high temperatures and pressures ($T > 250$°C and $P > 10$ atm). Key differences in both the qualitative and quantitative nature of the carboxylic acid and ammonia systems were sought.

Aqueous acid/base equilibrium calculations

Six species are central in the acid/base equilibria of the nitrile reaction mixtures: OH^-, H_3O^+, NH_3, NH_4^+, undissociated acid (HA), and dissociated acid (A^-). Their concentrations can be determined from the appropriate set of fundamental relations governing the acid/base equilibria of the system.

Several constraints assist in the solution of the equilibrium relations. The total carboxylic acid concentration (A_T) in the reaction mixture is known from measurements during the course of the reaction, and the reaction stoichiometry provides the total concentration of ammonia (N_T). This allows formulation of the two mass balance equations that relate the protonated and unprotonated forms of ammonia and acetic acid shown as Eqs. 4 and 5. The electroneutrality condition of Eq. 6 provides an additional constraint:

$$A_T = HA + A^- \quad (4)$$

$$N_T = NH_4^+ + NH_3 \quad (5)$$

$$[NH_4^+] + [H_3O^+] = [OH^-] + [A^-]. \quad (6)$$

The acid/base equilibria of the water, carboxylic acid, and ammonia provide the remaining relationships needed to specify the concentrations. These are summarized as dissociation equilibria in Eqs. 7–9, where the activity of water is assumed to be unity. The experimental values for K_W, K_A, and K_N given in Table 3 were available from the literature:

$$2H_2O \leftrightarrow OH^- + H_3O^+ \quad K_W = [OH^-][H_3O^+] \quad (7)$$

$$HA + H_2O \leftrightarrow A^- + H_3O^+ \quad K_A = \frac{[A^-][H_3O^+]}{[HA]} \quad (8)$$

$$NH_4^+ + H_2O \leftrightarrow NH_3 + H_3O^+ \quad K_N = \frac{[NH_3][H_3O^+]}{[NH_4^+]}. \quad (9)$$

In summary, the three equilibrium relations of Eqs. 7–9, the two mass balances of Eqs. 4 and 5, and the electroneutrality condition of Eq. 6 provide six constitutive relations for the calculation of the six unknown species concentrations. Thus, the system is completely specified. Additional manipulation of these equations provided Eq. 10 for the hydronium ion concentration as a function of the other measurable quantities:

$$[H_3O^+] + \frac{N_T[H_3O^+]}{K_N + [H_3O^+]} = \frac{K_W}{[H_3O^+]} + \frac{K_A A_T}{K_A + [H_3O^+]}. \quad (10)$$

This cubic expression for the hydronium ion concentration as a function of the total acid and total ammonia concentrations can be solved iteratively. Expressions for the concentrations of the other reaction species as a function of the hydronium ion concentration and the total acid and base concentrations are obtained from further manipulation of Eqs. 4 and 5 and Eqs. 7–9. The resulting relations given in Eqs. 11–14 are linear in the total acid or base concentration. Their overall behavior, however, is nonlinear due to the form of Eq. 10:

$$[HA] = \frac{A_T[H_3O^+]}{K_A + [H_3O^+]} \quad (11)$$

Table 3. Dissociation Constants at Ambient and Reaction Conditions

Reaction Conditions	pK_A Benzoic Acid*	pK_A Acetic Acid*	pK_N Ammonia**	pK_w Water†
$T = 25$°C, $P = 1$ bar	4.20	4.75	9.25	14.01
$T = 250$°C, $P = 40$ bar	—	6.01	5.43	11.40
$T = 300$°C, $P = 87$ bar	6.21	—	5.05	11.70

*Read, 1981.
**Read, 1982.
†Marshall and Franck, 1981.

$$[A^-] = \frac{A_T K_A}{K_A + [H_3O^+]} \tag{12}$$

$$[NH_4^+] = \frac{N_T [H_3O^+]}{K_N + [H_3O^+]} \tag{13}$$

$$[NH_3] = \frac{N_T K_N}{K_N + [H_3O^+]}. \tag{14}$$

These calculations allow a general characterization of the hydrolysis reaction environment, as follows.

Carboxylic acid and ammonia systems at 25 < T/°C < 300 and 1 < P/atm < 87

The pK_A values in Table 3 indicate that acetic acid and benzoic acid are relatively weak acids at ambient conditions and that ammonia is a base. The combination of carboxylic acid and ammonia (weak acid/weak base) in the present experiments forms the essential components of a buffer system. Figure 6 provides more quantitative information in terms of the results of equilibrium calculations for the addition of equimolar concentrations of carboxylic acid and ammonia to water at 25°C and 1 bar. For the acetic acid/ammonia system, $[H_3O^+]$ maintains the neutral value of 1.0×10^{-7} M as the equimolar concentration of acid and base increases. This is because the pK_A of acetic acid equals the pK_B for ammonia at ambient conditions. This is not the case for the benzoic acid/ammonia system, where the ratio of the benzoic acid pK_A to the ammonia pK_B is 0.88. This results in a range of buffer concentration where $[H_3O^+]$ increases with the equimolar acid/base concentration before reaching a constant value. An asymptotic value of 1.86×10^{-7} M is reached after addition of 1.2-mM benzoic acid and ammonia.

The pK_A values for both benzoic and acetic acid are higher at the reaction conditions of interest. This indicates a decrease in acidity. Figure 7 summarizes this information as a plot of the percent ionization (defined as the ratio of ionized acid, $[A^-]$, to the total acid, $[A_T]$) as a function of the total acid concentration. The percent ionization reaches an asymptotic value at high total acid concentrations. The decrease in acidity with increasing temperature is evident from the decrease in the asymptotic value of the percent ionization for both carboxylic acids at high temperatures and pressures. The percent ionization decreased from 18% to 4% for acetic acid (25°C and 250°C, respectively) and from 25% to 3% for benzoic acid (25°C and 300°C, respectively).

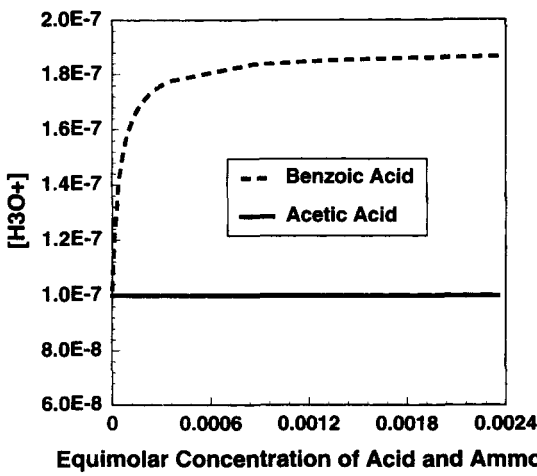

Figure 6. Buffer characteristics of carboxylic acid and ammonia system at ambient conditions (25°C, 1 bar).

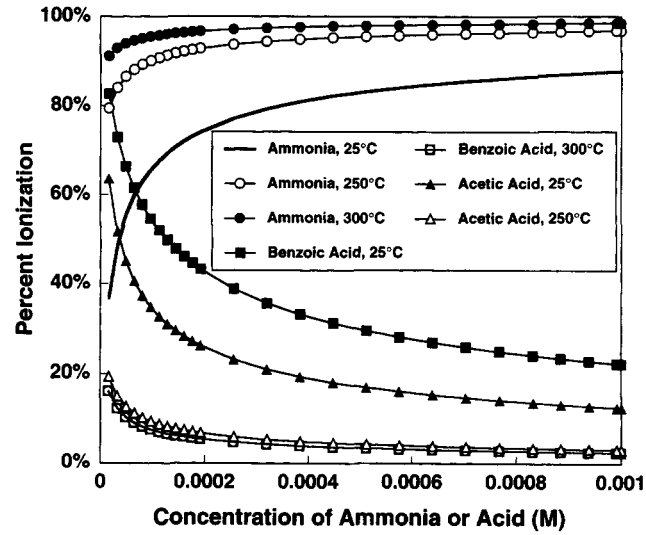

Figure 7. Variation of percent ionization with temperature and pressure for acetic acid, benzoic acid, and ammonia.

The pK_A of ammonia decreases with increasing temperature, characteristic of an increase in acidity. Figure 7 depicts the percent ionization of ammonia (NH_3/N_T) as a function of total ammonia (N_T) concentration and temperature. The increase in acidity of ammonia is evident from the increase in the asymptotic value of the percent ionization.

The pK_w for water decreases by nearly 2.5 orders of magnitude as the temperature and pressure increase from ambient to HTW conditions. This increases the ionic character of pure water, which contains equimolar concentrations of hydronium and hydroxide ions and defines the neutral concentration. Thus, the neutral concentration of hydronium ion increases from 1.0×10^{-7} M (pH 7) at ambient conditions to 2.0×10^{-6} M (pH 5.7) at 250°C and 40 bar. This effect, along with the normal Arrhenius effect, can be expected to influence the observed increase in the nitrile hydrolysis rate.

The net effect of the various changes in the individual dissociation constants with increasing temperature and pressure is small in the present system: the qualitative characteristics of the carboxylic acid/ammonia systems observed at room temperature remain. This scenario is developed in Figure 8 as a plot of hydronium ion concentration vs. the equimolar concentrations of acid and ammonia in the reaction system. Figure 8 simulates the physical chemistry of the nitrile and amide reaction environment, where time and buffer concentration have an implicit relationship through the reaction kinetics. It is worth emphasizing that the highest buffer concentrations obtained in the experiments were 0.85 M for acetonitrile and 0.72 M for benzonitrile. Figure 8 shows that the hydronium ion concentration reaches an asymptote for both acetic and benzoic acid at the HTW reaction conditions. For

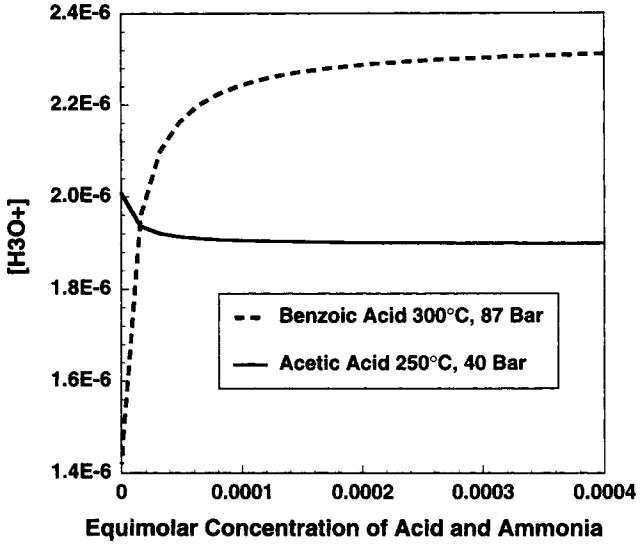

Figure 8. Buffer characteristics of carboxylic acid and ammonia system at high temperature and pressure.

the acetic acid/ammonia system, the hydronium ion concentration decreases slightly with increasing buffer concentration before reaching a value of 1.96×10^{-6} M. A larger change is observed for the benzoic acid/ammonia system, where the hydronium ion concentration increases to an asymptotic value of 2.3×10^{-6} M. The variations in Figure 8 are even less significant when considered in relation to the buffer concentrations reached in the experiments. The buffer concentrations yielding the asymptotes of Figure 8 are several orders of magnitude lower than the concentrations measured during the course of the nitrile hydrolysis. Thus, any kinetic effect of this transient hydronium ion concentration can be reasonably neglected in the kinetic modeling of this system.

In short, this analysis of the physical chemistry of the acid/ammonia systems has served to specify the essentially static value of $[H_3O^+]$. In addition, Eqs. 13–16 specify the concentrations of the remaining four species. As a consequence of the static hydronium ion concentration, the concentrations of NH_3, NH_4^+, HA, and A^- are linear functions of total acid concentration, A_T, or total base concentration, N_T.

Combined Kinetics and Solution Thermodynamics Model

Quantitative specification of the physical chemistry of the high-temperature water reaction environment allows solution of the reaction model. This, in turn, permits mechanistic analysis of the observed nonlinear kinetics for acetonitrile and benzonitrile hydrolysis. This will be developed here for nitrile hydrolysis, but it is also applicable to the reaction of amides.

The results shown in Figure 8 simplify the formulation of the governing rate constants, as the hydronium ion concentration attains an essentially constant value over the course of the experimental residence times. This suggests that the specific acid catalyzed rate constant, $k_{H_3O^+}$, can be lumped with the solvent-induced rate constant, k_1 of Eq. 2a. In addition, the large excess of water in the reaction mixture suggests that the system can be modeled isopicnic with respect to water. Equation 15 thus defines an apparent "solvent" hydrolysis rate constant:

$$k_1' \equiv k_1 + k_{H_3O^+}[H_3O^+]. \tag{15}$$

This leaves four potential catalytic species in Eq. 3: HA, A^-, NH_3, NH_4^+. The concentrations of these species are specified by Eqs. 11–14. The static H_3O^+ concentration allows further simplification of these relations. The result for HA is shown as Eq. 16, where the concentration of undissociated acid is a linear function of the total acid concentration and the proportionality constant, α_{HA}, is constant at buffer concentrations above 4 mM:

$$[HA] = \frac{[H_3O^+]}{K_A + [H_3O^+]} A_T = \alpha_{HA}(T,P)A_T. \tag{16}$$

The values of α_{HA} at reaction conditions of 300°C and 87 bar for acetic and benzoic acid are 0.86 and 0.79, respectively. Similar reasoning can be applied to Eqs. 11–14.

These simplifications allow representation of the effective rate constant of Eq. 17 in terms of the "solvent" and the "conversion-dependent" terms, the latter being represented by the total acid concentration:

$$k_{eff} = k_1' + \{k_{HA}\alpha_{HA} + k_{NH_4^+}\alpha_{NH_4^+} + k_A\alpha_A + k_{NH_3}\alpha_{NH_3}\}A_T. \tag{17}$$

Equation 17 invites a simpler representation of the rate constant in terms of one effective parameter that accounts for the uncatalyzed rate, k_1', and another, k_3', that accounts for the general acid/base catalysis, where $k_3' = k_{HA}\alpha_{HA} + k_{NH_4}\alpha_{NH_4} + k_A\alpha_A + k_{NH_3}\alpha_{NH_3}$.

This logic provided rate laws for the governing reaction network of Figure 5. Catalytic activity was attributed to the total acid produced in the secondary hydrolysis of the amide. Rate constants k_1' and k_2' accounted for the solvent-induced hydrolysis of the nitrile and amide, respectively. Rate constants k_3' and k_4' are the general acid/base catalysis constants, and k_5' accounts for the reversibility of the amide hydrolysis step. The foregoing analyses and simplifications results in the following rate law for nitrile disappearance:

$$-r_{Nitrile} = k_1'[R-CN] + k_3'[A_T][R-CN] \tag{18}$$

Likewise, for the amide disppearance, the rate law was:

$$-r_{Amide} = k_2'[R-C(O)NH_2] + k_4'[A_T][R-C(O)NH_2] - k_5'[A_T][R-C(O)OH][NH_3]. \tag{19}$$

Optimization of kinetic parameters

Optimal values of the five rate constants were determined through the use of the multilevel single linkage (MLSL) algorithm (Stark, 1993). This global optimization method randomly chooses points within the parameter space at which

Table 4. Optimized Rate Constants for the Reaction of Nitriles and Amides in HTW

Reaction Temp. (°C)	Reactant	k_1 Nitrile Hydrolysis (min^{-1})	k_2 Amide Hydrolysis (min^{-1})	k_3 Nitrile Catalyzed ($M^{-1}\cdot min^{-1}$)	k_4 Amide Catalyzed ($M^{-1}\cdot min^{-1}$)	k_5 Amide Reversible ($M^{-2}\cdot min^{-1}$)
300	Benzonitrile/ benzamide	7.44×10^{-3}	1.15×10^{-2}	1.35×10^{-1}	1.72×10^{-1}	1.70×10^{-1}
300	Acetonitrile	3.38×10^{-3}	2.80×10^{-2}	6.61×10^{-2}	4.63×10^{-1}	5.43×10^{-1}
250	Acetamide	—	4.79×10^{-3}	—	8.16×10^{-2}	6.84×10^{-2}

the objective function is evaluated. Subsequently, a local minimization procedure is started at 10% of the randomly chosen points having the lowest objective function values. The local minimum with the smallest objective function value is taken as the global minimum.

The objective function was a variation of the sum of square errors shown in Eq. 20, where F is the value of the objective function, and y_{ij}^{pred} and y_{ij}^{exp} are the predicted and measured molar yields for species i at time j, respectively. The weighting factor (w_i) was specified as the inverse of the standard error associated with the measurement of a particular component, thus making the model predictions most sensitive to the components measured with the best precision:

$$F = \sum_{j=1}^{\#\text{ times}} \sum_{i=1}^{\#\text{ comp}} w_i\left(y_{ij}^{pred} - y_{ij}^{exp}\right)^2. \qquad (20)$$

A subset of each nitrile reaction network was realized in the reaction of the corresponding amide. In this case, only amide, ammonia and acid were present in the system. These experiments allowed estimation of the rate constants k_2, k_4, and k_5.

The parameter estimation results are summarized in Table 4, and the model fits for benzonitrile and acetonitrile are given in Figures 2a and 2b, respectively. The predicted molar yields for both nitriles are in excellent agreement with experimental values, with the average deviation being 1.5% for benzonitrile and 2.0% for acetonitrile. For acetonitrile, a systematic underprediction of the experimental acetic acid yields is evident at long residence times. This deviation is attributed to analytical difficulties in measuring high carboxylic acid concentrations via gas chromatography. The measured experimental acid concentrations at these residence times resulted in mole balances greater than 100%.

Discussion

Several differences and similarities in the reactivities of acetonitrile and benzonitrile are apparent from the optimal rate constants in Table 4. Rate constants for both catalyzed and uncatalyzed steps for benzonitrile hydrolysis are a factor of 2 larger than those for acetonitrile hydrolysis. Figure 9 probes the role of autocatalysis in nitrile hydrolysis as a plot of the catalyzed rate divided by the total rate of nitrile hydrolysis vs. nitrile conversion. In addition, a simulated curve for benzonitrile at 0.71-M initial concentration using the rate constants of Table 4 is included for comparison. Autocatalysis is clearly more important in acetonitrile hydrolysis, particularly at low conversions. At 20% conversion the fraction of the catalyzed acetonitrile hydrolysis rate is nearly 0.65, while the fraction of catalyzed benzonitrile hydrolysis is 0.24. This difference is attributed to the lower reactivity of the benzamide relative to acetamide, which results in lower acid (catalyst) concentrations. Figure 9 also shows that the fraction of catalyzed nitrile hydrolysis is a function of the initial nitrile concentration .

Marked differences were observed for the reactivity of the aliphatic and aromatic amides. For acetamide, both the catalyzed and uncatalyzed amide reactivity is significantly higher than that of the nitrile. The ratios of the amide-to-nitrile rate constants were 8.3 and 7.0 for the uncatalyzed and catalyzed steps, respectively. The difference in uncatalyzed benzonitrile reactivity is less pronounced. The rate constants for the uncatalyzed hydrolysis of benzonitrile and benzamide are nearly equal. The ratio of catalyzed amide to catalyzed nitrile hydrolysis is less than one, indicating a higher reactivity for the nitrile. The chemical explanation of these results may lie in the accepted mechanism for amide hydrolysis, in which a tetrahedral intermediate is formed. Steric effects may hinder the formation of this intermediate during benzamide hydrolysis (McMurry, 1984).

Implications of Autocatalysis

Autocatalytic reaction networks lead to anomalous kinetic behavior, which can influence decisions concerning the optimal reactor configuration to achieve specified design goals in the application of reactions in HTW. Two such applications

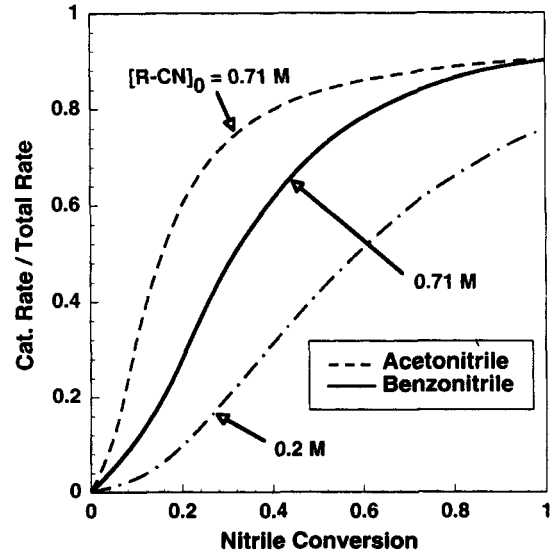

Figure 9. Comparison of catalyzed nitrile hydrolysis rates in HTW.

are evident. One is the remediation of dilute, aqueous waste streams. In this case, the primary design criterion is the overall conversion of a toxic material to more benign forms. The second is chemical production. Here, the focus is the production of an intermediate or end product in the reaction network. The implications of autocatalysis with regard to the preceding applications are discussed in the context of the present experimental conditions and results.

Kinetics aspects of autocatalysis

The kinetic implications of autocatalysis can be illustrated by manipulation of the rate law of Eq. 18, which can be written as:

$$-r_{\text{Nitrile}} = [\text{R}-\text{CN}](k'_1 + k'_3[\text{R}-\text{CN}]_0 y_{\text{acid}}), \qquad (21)$$

where $[\text{R}-\text{CN}]_0$ is the initial nitrile concentration, and y_{acid} is the yield of acid ($[A_T]/[\text{R}-\text{CN}]_0$). The yield of acid varies from zero to near one during the reaction, with the final value determined by thermodynamics. The relative magnitudes of the terms k'_1 and k'_3 $[\text{R}-\text{CN}]_0 y_{\text{acid}}$ determine the extent of autocatalysis present in the system. Initially, the nitrile systems behave as first order since y_{acid} is zero. If the term k'_3 $[\text{R}-\text{CN}]_0 y_{\text{acid}}$ is small compared to k'_1, the system will always behave as first order. The form of Eq. 21 clearly emphasizes the importance of initial reactant concentration in HTW hydrolysis of nitriles.

The technology of aqueous stream remediation by hydrolysis suggests that the initial concentration effect will be one of the key process design considerations. As the initial concentration of nitrile increases, the autocatalytic nature of the system becomes more important. The dependence of nitrile conversion kinetics on initial concentration is shown in Figure 10 for acetonitrile and benzonitrile. Low initial concentrations exhibit nearly first-order kinetics, while high initial concentrations show noticeable autocatalytic behavior. Benzonitrile hydrolysis rates are higher than those for acetonitrile up to initial concentrations of > 5 M, where the rates become comparable. Figure 10 also shows that the acetonitrile reaction rate increases faster with initial nitrile concentration than does the benzonitrile rate. This results from a faster time evolution of y_{acid} for acetonitrile relative to benzonitrile.

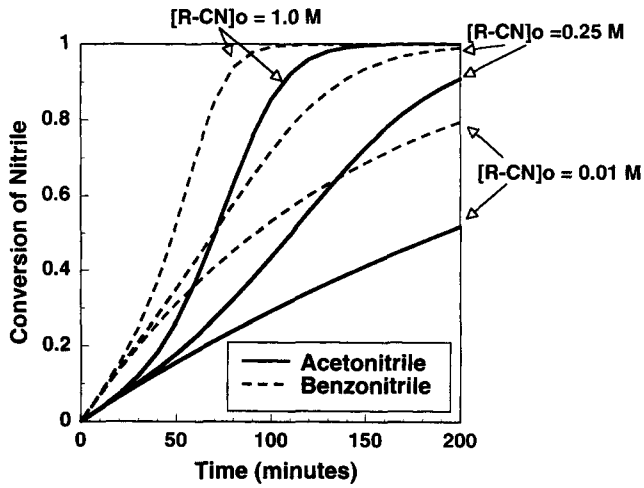

Figure 10. Model predictions of nitrile conversion at various initial reactant concentrations.

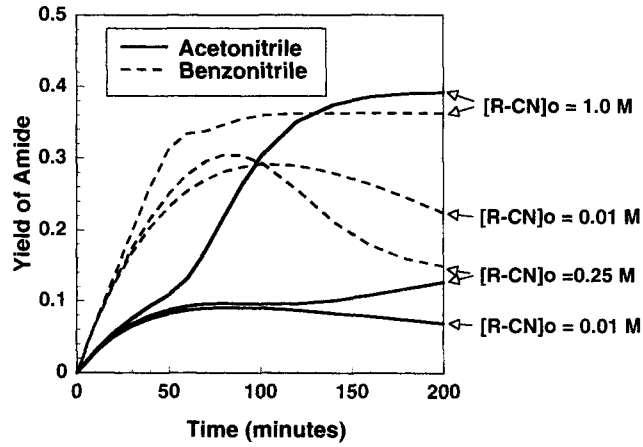

Figure 11. Amide yield behavior as a function of initial nitrile concentration.

Chemical process technology for recovery of products could engender different design considerations. Maximizing the production of the intermediate amide for this system requires special attention to the reaction kinetics. The highest amide yield is obtained with high initial nitrile concentration and high conversion. Low initial nitrile concentrations require intermediate conversions to maximize amide selectivity. These scenarios are depicted in Figure 11 as a plot of the time evolution of the amide yield for various initial nitrile concentrations.

Reactor design considerations

Various reactor design scenarios brought about by the autocatalytic kinetics are compared in Figure 12 as a plot of

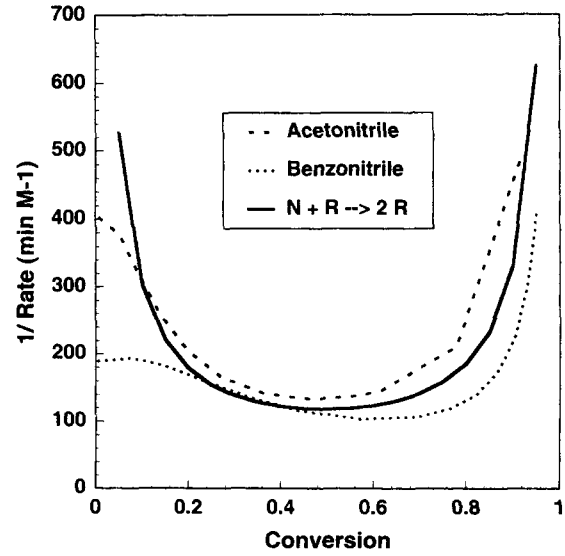

Figure 12. Rate behavior of " zero initial rate" autocatalytic system and autocatalytic nitrile hydrolysis at 300°C and 87 bar.

inverse rate vs. conversion. Recall that the area under the curve is proportional to the PFR volume required for a given conversion, whereas the area of the 1/(rate)–conversion rectangle is proportional to the CSTR volume. The profiles of Figure 12 were generated using the optimized model at conditions relevant to the present experiments: the initial concentration of reactants was 0.71 M and the reaction was run at 300°C and 87 bar. For comparison, the "zero initial rate" autocatalytic model $N + R \rightarrow 2R$ (Levenspiel, 1972; Hill, 1977; Froment and Bischoff, 1990), with $R_0 = 0.0071$ M is also shown in Figure 12. The catalytic rate constant for the reaction of acetonitrile found in Table 4 served as the rate constant for the "zero initial rate" autocatalytic reaction.

In Figure 12, all three systems pass through a minimum in 1/(rate) vs. conversion, which approaches infinity at high conversion. A key difference is observed in the low conversion limit for the acetonitrile and benzonitrile systems. These systems assume a finite value of 1/(rate) in the limit of low conversion. This finite rate is a result of the parallel, solvent-induced (uncatalyzed) hydrolysis of the nitrile. In contrast, the zero initial rate autocatalytic scheme obtains a large value at lower conversion due to the low concentration of catalyst in this region. The presence of the minimum in these plots directs the choice of reactor type for specified conversions. Low-to-intermediate conversions dictate a CSTR to provide the minimum reactor volume. At higher conversions, however, a PFR becomes the single optimal reactor. Clearly, CSTR–PFR combinations can have advantages as well.

The autocatalytic nature of the nitrile hydrolysis system and the associated reactor design considerations depends greatly on the initial concentration of nitrile. To probe this issue, Figure 13 illustrates the dependence of $[R{-}CN]_0$/rate on conversion for varying initial benzonitrile concentrations. The rate was normalized by $[R{-}CN]_0$, as per Eq. 22, to allow comparison of holding times:

$$\tau = \int_0^X \frac{[R{-}CN]_0}{-r_N} dx. \tag{22}$$

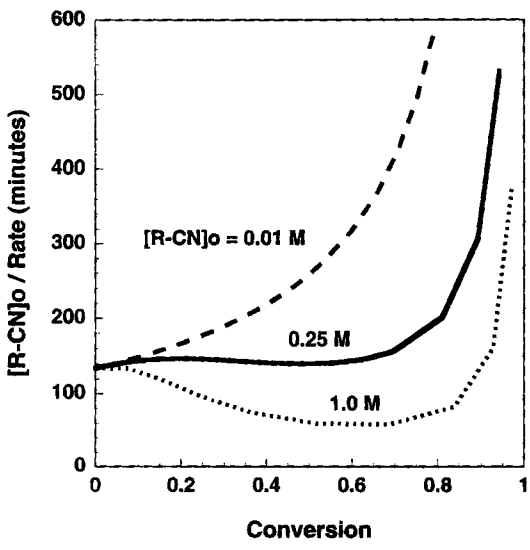

Figure 13. Consequence of initial concentration dependence on reactor design scenarios.

For an initial concentration of 1.0 M and conversion of 70% (corresponding to the minimum $[R{-}CN]_0/r_N$), the optimal reactor is a CSTR. As the initial concentration of benzonitrile decreases, the minimum in the $[R{-}CN]_0/r_N$ profile diminishes. At an initial concentration of 0.25 M, the volumes of a CSTR and PFR are comparable for 70% conversion. Conversions higher than 70% at this initial concentration dictate the use of a PFR. The minimum vanishes entirely at initial concentrations approaching 0.01 M. At these concentrations, a PFR is the optimal reactor independent of desired conversion.

In summary, autocatalytic kinetics lead to reactor design opportunities and challenges. In particular, the minimum reactor volume to achieve a desire conversion is strongly influenced by autocatalytic kinetics. The initial concentration of a reactant requires special attention for the autocatalytic reaction scheme for nitrile hydrolysis. To a large extent, the initial reactant concentration governs the qualitative rate behavior, which in turn influences the optimal reactor configuration for either a minimum required volume or a maximum yield of the intermediate amide.

Conclusions

1. The overall reactivities of acetonitrile and benzonitrile at 300°C and 87 bar were comparable. Both reactants displayed characteristics of autocatalytic kinetics.

2. Clean product spectra dominated by amides and carboxylic acid were observed for both reactants. No decarboxylation of the acid was observed.

3. The reaction of the amide to carboxylic acid was found to be reversible, with the equilibrium favoring the acid product.

4. The rate of nitrile hydrolysis was directly proportional to the concentration of carboxylic acid.

5. Both the acetic acid/ammonia and benzoic acid/ammonia systems displayed characteristics of a buffer system at high temperature and pressures, which results in a constant hydronium ion concentration (pH) during the course of the nitrile reaction. This further supported the direct role of reaction products in the conversion of the nitrile and amide and aided in development of a pathway-level model that captures the kinetic behavior of the system.

6. A five-step reaction network captured the key features of the reaction of nitriles at 300°C and 87 bar. Equilibrium relations were implemented to relate the model parameters to the total acid concentration. This resulted in an effective autocatalytic rate constant for both nitrile and amide hydrolysis. Optimization of the rate parameters yielded excellent model fits to experimental data. Key differences in the catalyzed and uncatalyzed rate constants for acetonitrile and benzonitrile were observed. Most importantly, the aromatic amide reactivity is significantly lower than the aliphatic reactivity for both catalyzed and uncatalyzed cases. This, in turn, determines the overall importance of catalysis in nitrile hydrolysis. The lower aromatic amide reactivity diminishes the autocatalytic effect.

7. The presence of autocatalysis in nitrile hydrolysis leads to anomalous rate behavior. In particular, the qualitative pattern of kinetics was sensitive to the initial concentration of the reactant. This in turn, can influence the choice of reactor configuration to achieve a desired design objective.

Acknowledgments

We are grateful to the Army Research Office/University Research Initiative for financial support of this research, and Professor Keith Johnston at University of Texas for helpful technical discussions.

Notation

$[x]$ = concentration in molar units
K_W = ionization constant of water
K_A = acidity constant for acid
K_N = acidity constant for ammonia
k_1 = first-order nitrile to amide hydrolysis rate constant
k_2 = first-order amide to acid hydrolysis rate constant
k_3 = second-order acid catalyzed nitrile hydrolysis rate constant
k_4 = second-order acid catalyzed amide hydrolysis to rate constant
k_5 = third-order acid catalyzed reversible amide rate constant
k_i' = pseudo-rate-constant containing water concentration

Literature Cited

Froment, G., and K. B. Bischoff, *Chemical Reactor Analysis and Design*, Wiley, New York (1990).

Grigoryan, E. P., G. F. Vytnov, R. N. Rodyukova, and N. V. Ipatovia, "Hydrolysis of Acrylonitrile to Acrylamide," *J. Appl. Chem. USSR*, **48**, 2044 (1976).

Hill, C. G., Jr., *Introduction to Chemical Engineering Kinetics and Reactor Design*, Wiley, New York (1977).

Iyer, S. D., G. R. Nichol, and M. T. Klein, "Hydrothermal Reactions of 1-Nitrobutane in High Temperature Water," *J. Supercrit. Fluids*, **9**, 26 (1996).

Katritzky, A. R., A. R. Lapucha, and M. Siskin, "Aqueous High-temperature Chemistry of Carbo- and Heterocycles. 12. Benzonitriles and Pyridinecarbonitriles, Benzamide and Pyridinecarboxamides, and Benzylamides and Pyridylamines," *Energy Fuels*, **4**, 555 (1990).

Krieble, V. K., and C. I. Noll, "The Hydrolysis of Nitriles with Acids," *JACS*, **61**, 560 (1939).

Kuhlmann, B., E. M. Arnett, and M. Siskin, "Classical Organic Reactions in Pure Superheated Water," *J. Org. Chem.*, **59**, 3098 (1994).

Levenspiel, O., *Chemical Reaction Engineering*, Wiley, New York (1972).

Loudon, G. M., *Organic Chemistry*, Benjamin/Cummings, Menlo Park, CA (1988).

March, J., *Advanced Organic Chemistry Reactions, Mechanisms, and Structure*, Wiley, New York (1992).

Marshall, W. L., and E. U. Frank, "Ion Product of Water Substance, 0–1000°C, 1–10,000 bar: New International Formulation and Its Background," *J. Phys. Chem. Ref. Data*, **10**(2), 295 (1981).

McMurry, J., *Organic Chemistry*, Brooks/Cole, Monterey, CA (1984).

Rabinovitch, B. S., and C. A. Winkler, "The Hydrolysis of Aliphatic Nitriles in Concentrated Hydrochloric Acid Solutions," *Can. J. Res.*, **20**(Sec. B), 221 (1942a).

Rabinovitch, B. S., and C. A. Winkler, "Kinetics of the Alkaline Hydrolysis of Propionitrile," *Can. J. Res.*, **20**(Sec. B), 185 (1942b).

Rabinovitch, B. S., C. A. Winkler, and A. P. R. Stewart, "The Hydrolysis of Propionitrile in Concentrated Hydrochloric Acid Solutions," *Can. J. Res.*, **20**(Sec. B)(7), 121 (1942).

Read, A. J., "Ionization Constants of Aqueous Ammonia from 25 to 250°C and to 2000 Bar," *J. Solution Chem.*, **11**(9), 649 (1982).

Read, A. J., "Ionization Constants of Benzoic Acid from 25 to 250°C and to 2000 Bar," *J. Solution Chem.*, **10**(7), 437 (1981).

Stark, S. M., "An Investigation of the Applicability of Parallel Computation to Demanding Chemical Engineering Problems," PhD Diss., Univ. of Delaware, Newark (1993).

Wideqvist, S., "The Alkaline Hydrolysis of Acetonitrile," *Ark. Kemi*, **10**, 256 (1956).

Manuscript received Oct. 15, 1996, and revision received Apr. 14, 1997.